On-chip cell labelling and washing by capture and release using microfluidic trap arrays

Yu Chen,[1,2] Robert H. Austin,[1,3] and James C. Sturm[1,2]
[1]*Princeton Institute for Science and Technology of Materials (PRISM), Princeton, New Jersey 08544, USA*
[2]*Department of Electrical Engineering, Princeton University, Princeton, New Jersey 08544, USA*
[3]*Department of Physics, Princeton University, Princeton, New Jersey 08544, USA*

(Received 31 May 2017; accepted 12 September 2017; published online 27 September 2017)

Flow cytometry analysis requires a large amount of isolated, labelled, and purified cells for accurate results. To address the demand for a large quantity of cells prepared in a timely manner, we describe a novel microfluidic trap structure array for on-chip cell labelling, such as intracellular and extracellular labelling, and subsequent washing and release of cells. Each device contains 7×10^4 trap structures, which made the preparation of large numbers of cells 3×10^5 possible. The structure has a streamlined shape, which minimizes clogging of cells in capture and release steps. The trap structure arrays are built and tested using leukocytes, with different load flow speeds, incubation times, and release flow speeds. ~85% of cells are captured independent of the input flow speed. The release efficiency depends on the incubation time, with over ~80% of captured cells released for up to 20 min incubation, and on-chip labelling and washing with STYO13 are demonstrated. Qualitative models are developed as guidance for designing the proposed trap structure and to explain the increased performance over previous approaches. *Published by AIP Publishing.* [http://dx.doi.org/10.1063/1.4985771]

INTRODUCTION

The analysis of biological cells, such as leukocytes, erythrocytes, and circulating tumour cells (CTCs), involves many chemical processes of cells (such as labelling with monoclonal antibodies and a fixation/permeabilization step). These chemical processes are typically followed by a washing step to remove the unbound labels or excess chemicals from the processed cells to yield processed and washed cells. Both the chemical process and washing step usually require multiple manual steps, for example, pipetting, centrifugation, and resuspension of a pellet after centrifugation. These labor-intensive steps will inevitably cause variations and introduce artifacts to the quality of processed cells and the results of subsequential analysis or diagnosis.[1]

For more uniformly processed cell samples, automated and integrated processing and preparation of cells are preferred. Nguyen *et al.* have presented a PDMS-based microfluidic system for on-chip whole blood cell count and preparation from raw blood,[2] which has a complicated design of multiple functional sections and needs accurate fluid controls to function correctly, limiting its practicality. Simpler microfluidic structures that can be easily integrated for high-throughput applications such as "centrifuge-on-a-chip"[3] and deterministic lateral displacement (DLD) arrays[4] have shown potential in specific domains but have major drawbacks. The former is limited by low cell capture efficiency: 80% to 90% of the inputted cells are lost due to the underlying capture mechanism, which thus requires extra cell enrichment and purification steps for rare cell applications. The latter provides only ~100 ms – 2 s of on-chip incubation to yield a low desired level of contamination of the output by processing chemicals such as labels.[4,5] Therefore, there is a need for an approach that can recover most of the inputted cells, provide long on-chip incubation, and be practical for a broad range of cell analysis applications.

Towards this goal, Huebner *et al*. have demonstrated a simple 2-dimensional trap structure for droplet trapping, incubation, and release for enzymatic and cell-based assays.[6] 90% of captured droplets can be released from the trap structure although the capture efficiency is extremely low: >90% of inputted droplets just pass through the trap array. 2-dimensional traps were also used extensively for single cell capturing and analysis.[7–9] A 3-dimensional trap structure of a similar idea is proposed by Di Carlo *et al*. for on-chip cell culture and single-cell analysis for enzyme concentrations, kinetics, and inhibition.[10,11] Again the capture efficiency of cells is still very low. Interestingly, a modified 3-dimensional trap structure has shown a cell capture efficiency of ~90%.[12] However, the reason for the improvement of capture efficiency is not clear, and this 3-dimensional trap structure is not capable of cell release for further off-chip chemical processing and/or analysis, such as lysis and DNA sequencing. Some cell analysis technologies, such as flow cytometry and Coulter counting, usually require large amounts of cells (10^4 to 10^6) to be analyzed for accurate results, which demand both high capture and release efficiency.

Inspired by these works, we demonstrate a novel 3-dimensional microfluidic trap structure array which can be used for subsequent on-chip chemical processing of captured cells, washing, and then release for off-chip characterization [Fig. 1(a)]. Each device has 7×10^4 traps, which is suitable to prepare a large quantity of target cells in a timely manner. There is a critical gap G_C between the trap structure and a planar lid on top of the chip. When cells larger than the critical gap move into the traps, they will be physically captured due to their size. On the other hand, when a flow applied from the other direction, a fluidic force along the flow direction will push the cells out of the trap structure. Particles or cells can be captured [Fig. 2(a)], labeled (or processed by other chemicals) [Fig. 2(b)], washed [Fig. 2(c)], and released [Fig. 2(d)] for further analysis and process.

MATERIALS AND METHODS

Microfluidic device design

Figure 1(b) displays the top view schematic of the microfluidic trap array. In our experiments, the open region of the trap structure is $W_1 = 18\,\mu\text{m} \times L_1 = 15\,\mu\text{m}$, which is large to capture most leukocytes (10 to 20 μm diameter[13]), circulating tumor cells (CTCs, 8 to 20 μm

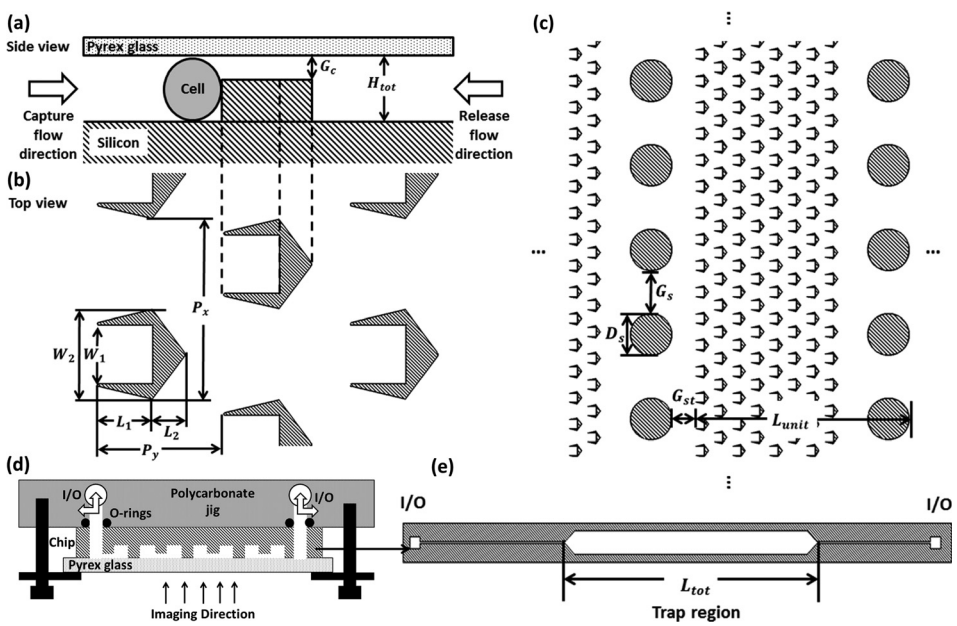

FIG. 1. (a) Side view schematic of the trap structure, with a critical gap G_C between the trap to the Pyrex glass lid in a channel of H_{tot} height. (b) Top view: $P_x = 50\,\mu$m and $P_y = 35\,\mu$m. (c) Each device unit ($L_{unit} = 450\,\mu$m long) consists of 1 column of support pillars and 8 columns of microfluidic traps. (d) Schematic of the experimental setup. (e) Each device of width 2 mm contains 53 device units, providing 7×10^4 traps and 2.8×10^5 traps for four devices in parallel.

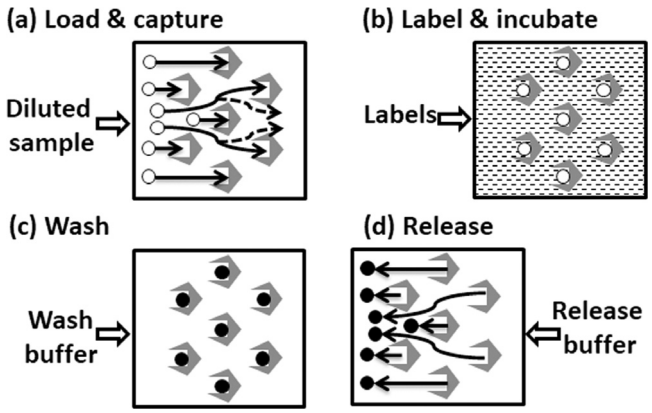

FIG. 2. Operations for on-chip labelling of biological cells using the proposed microfluidic device: (a) Load the cell sample to the device and physically capture the cells. (b) Input the process chemical (labels) to the device and incubate. (c) Rinse with wash buffer to remove the unbound labels. (d) Release the processed cells from the device.

diameter[14,15]), etc. An isosceles triangle of $L_2 = 10\,\mu$m height and $W_2 = 25\,\mu$m base is placed next to the open region to reduce clogging during the release step. The entire trap structure fits a square of $25\,\mu$m edge. The trap array has a $P_x = 50\,\mu$m spacing in the x-direction and a $P_y = 10\,\mu$m spacing in the y-direction. Each device unit, $L_{unit} = 450\,\mu$m long, consists of 1 column of support pillars for the lid and 8 columns of microfluidic traps. The support pillars are circular posts of $D_s = 80\,\mu$m diameter, $G_s = 80\,\mu$m gap between each two posts, and a $G_{st} = 50\,\mu$m gap to the trap array. The purpose of support pillars is to avoid the deformation of the Pyrex glass lid (anodically bonded to the pillars and channel walls) to maintain tight control of the critical gap across the device channel. Four devices [Fig. 1(e)] were used in parallel in each experiment. Each device of width 2 mm contains 53 device units, providing 7×10^4 traps and 2.8×10^5 traps for four devices in parallel.

Device fabrication and operation

Devices with a critical gap (G_C) of $6\,\mu$m were fabricated in silicon wafers using standard microfabrication techniques. Two-step Deep Reactive Ion Etching (DRIE) was performed to construct the 3-dimesnional microfluidic trap structure. Etching masks were formed on the silicon wafers using single-layer photolithography (Karl Suss, MA6) with an AZ 1518 photoresist (AZ Electronic Materials, USA) and an AZ 300 MIF developer. Samples were then anisotropically etched to $14\,\mu$m deep using a Samco RIE800iPB for first DRIE. A second DRIE was performed via the same photolithography procedure to create the $6\,\mu$m critical gap (Figs. 1 and 2 in the supplementary material). The microfluidic trap structures can also be fabricated with PDMS for low-cost and practical mass production. This requires a mold, microfabricated in silicon. Furthermore, high-resolution and high-accuracy soft lithography technologies are required to achieve the rigid microstructures with well-controlled resolution in horizontal (x, y) and vertical (z) directions, which is still relatively difficult compared to silicon fabrication technologies. Inlets and outlets are through-wafer holes created by sandblasting using $50\,\mu$m diameter aluminum oxide particles (PrepStart, Danville Engineering). Finally, the fabricated devices with the traps and support pillars were sealed with Pyrex glass (Dell Optics Co., Inc.) by anodic bonding techniques after Piranha and hydrofluoric acid clean.[16] The devices were mounted to a polycarbonate jig [Fig. 1(d)] connected to an external syringe pump (Fusion 400, Chemyx, USA). $0.2\,\mu$m polytetrafluoroethylene (PTFE) filters were applied to the jig to allow air to be pushed out of the manifold. A stainless steel metal plate with a window for microscopic observation was used to support the devices and the polycarbonate jig.

An inverted microscope (Nikon Eclipse Ti) was used to image the capture, labelling, and release of cells or particles in the devices, with high pressure mercury lamp as an excitation source with a matching fluorescence filter set (FITC, 467–498 nm excitation and 513–556 nm

emission). Images and movies were recorded with a 20X Nikon plan fluorite imaging objective (0.50 NA and 2.1 mm WD) using a CoolSNAP ES2 CCD camera and Micro-Manager software.

In each experiment, the devices were first rinsed and wet with a degassed 0.2% Pluronic F108 surfactant in deionized water and then the wash buffer (see later). Next, the sample solution (stained or unstained leukocytes or polystyrene beads) and label solution were sequentially loaded into the syringe pump and driven through the microfluidic system. After these two steps, wash buffer was applied in the same direction to remove the unbound labels, thus reducing the background noise of the processed sample. Pipettes were then used to collect all the remaining liquids in the input and output reservoirs to avoid contamination in the release step. Finally, release buffer was inputted from the other direction (the outputs of previous steps) to release the captured, labelled, and washed sample to the collection reservoirs (the inputs of previous steps).

For consistency, an average flow velocity in the device (v_{avg}) is used to represent all simulation and experimental results, where v_{avg} is defined as

$$v_{avg} = \frac{L_{tot}}{\tau} = \frac{L_{tot}F}{V_{tot}}, \tag{1}$$

where $L_{tot} = 2.4\,\text{cm}$ is the total length of the device channel, $\tau = V_{tot}/F$ is the average residence time for the fluid to flow through the device channel, F is the volume flow rate of the syringe pump, $V_{tot} = nL_{tot}W_{tot}H_{tot}\theta$ is the total fluid volume of the device channel, $n = 4$ is the number of devices used, $W_{tot} = 2\,\text{mm}$ and $H_{tot} = 20\,\mu\text{m}$ are the total width and the depth of the device channel, respectively, and θ is the "void fraction," i.e., the fraction of the array volume filled with fluid (i.e., excluding the traps and support pillars). For the device with critical gap $G_C = 6\,\mu\text{m}$, $\theta \approx 0.91$. For our syringe pump flow rates ranging from 0.4 μl/min to 80 μl/min, the average flow speed ranges from 46 μm/s to 9.2 mm/s.

Preparation of experimental samples

The wash buffer and release buffer were 1% Kolliphor P 188 (purchased from Sigma-Aldrich, Inc.) and 7 mM Ethylenediaminetetraacetic Acid (EDTA) in Phosphate buffered Saline (PBS) buffer. Venous EDTA-anticoagulated blood (purchased from Interstate Blood Bank, Inc., Memphis, TN, USA) was first 1:10 mixed with 1× RBC Lysis Buffer (eBioscience, Inc.) and incubated at 4 °C for 30 min to lyse red blood cells. The solution was then centrifuged at 2000 × g for 20 min, and the pellet (mostly leukocytes) was collected and diluted with the wash buffer to form a final concentration of about 2×10^5 cells/ml. This solution served as the unstained leukocyte sample solution in the following experiments. The stained leukocyte sample solution was prepared using the same protocol, except that the blood as purchased was first 200:1 stained with SYTO 13 (Thermo Fisher Scientific Inc.) for 10 min at room temperature. The bead sample solution was 10 μm Fluoresbrite YG Microspheres (Polysciences, Inc.) 1:500 diluted with the wash buffer, with a final concentration of about 8×10^4 particles/ml. The label solution was SYTO 13 as purchased and 1:200 diluted with wash buffer. The final concentration is about 25 μM.

RESULTS AND DISCUSSION

Leukocyte capture

For leukocyte experiments, four 6 μm critical gap devices were used. Deformation of cells in shear flow enables them to pass through 8 to 10 μm gaps,[17] and some cells of diameter ~20 μm will get stuck if the critical gap is too small. RBC-lysed SYTO13-stained leukocyte solutions of 2×10^5 cells/ml concentration were loaded at an average flow speed of 46 μm/s, 460 μm/s, or 4.6 mm/s for 5 min. Figure 3(a) shows the time sequence of leukocyte capture at an average flow speed of 460 μm/s (movie M1 in the supplementary material). The images are 10 s apart with an exposure time of 10 ms. From the capture experiments, we can see that most traps

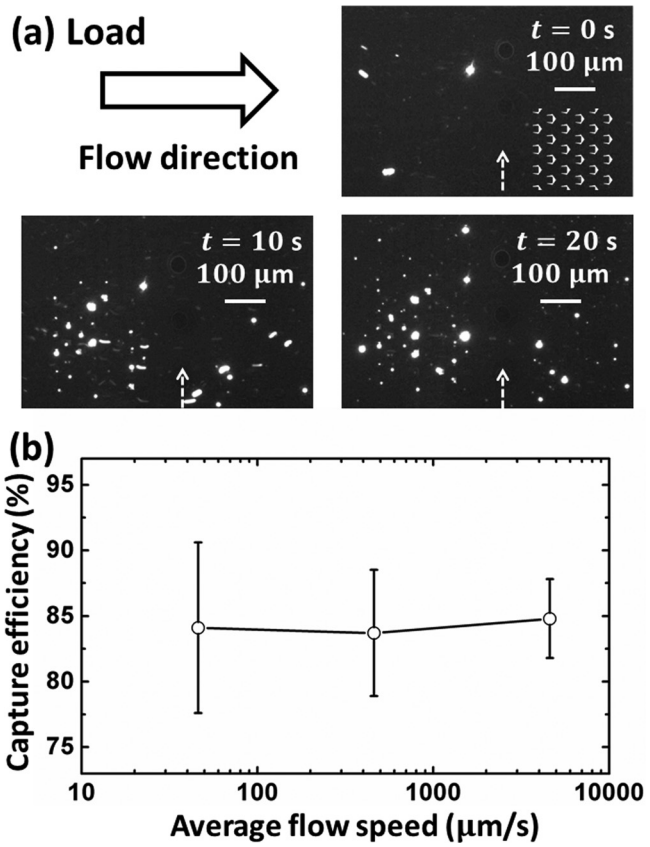

FIG. 3. (a) Time sequence of leukocyte capture at an average flow speed of 460 μm/s (movie M1 in the supplementary material). A pre-stained leukocyte sample solution was used. The top right image shows the outlines of the traps. (b) Experimental capture efficiency of leukocytes in devices with 6 μm critical gap at different flow speeds. Input speeds of 46 μm/s, 460 μm/s, and 4.6 mm/s had 5, 20, and 100 experiments, respectively. Each experiment was conducted via inputting 0.7 μl leukocyte sample solution and then counting the number of escaping leukocytes at the outputs. The dashed arrows point out the location of the row of support pillars. The stripes in the time sequence micrographs are the time-lapse traces of the cells due to the 10-ms exposure time.

capture approximately one cell at a time. Figure 3(b) shows the experimental results of the capture efficiency of devices with 6-μm critical gap of different flow speeds, measured as 1-n_{escape}/n_{tot}, where n_{escape} is the number of leukocytes passing through the device and n_{tot} is the number of total inputted leukocytes. Input speeds of 46 μm/s, 460 μm/s, and 4.6 mm/s had 5, 20, and 100 experiments, respectively. Each experiment was conducted by inputting 0.7 μl stained leukocyte sample solution and then counting the number of escaping leukocytes at the outputs. The capture efficiencies were 84.1%, 83.7%, and 84.8% for input speeds of 46 μm/s, 460 μm/s, and 4.6 mm/s, respectively, almost as high as the 90% in Ref. 12. The increased input speed did not have a significant impact on the leukocyte capture efficiency.

SYTO13 leukocyte labelling and washing

An unstained leukocyte sample solution was first inputted at 460 μm/s for 5 min to trap cells. A diluted SYTO13 labelling solution (25 μM), a nucleic acid stain, was then loaded to the device at 460 μm/s. Figures 4(a)–4(c) show the time sequence of leukocyte on-chip labelling with SYTO13 (movie M2 in the supplementary material). The images were taken at $t = 0$ s, when labelling solution just arrived in the observed region, $t = 20$ s, and $t = 50$ s, respectively, with an exposure time of 10 ms. Note that some cells were labelled with more SYTO13 (brighter than the other cells), which can be attributed to the various types of leukocytes, such as leukocytes, monocytes, and granulocytes. To differentiate the types of the trapped cells,

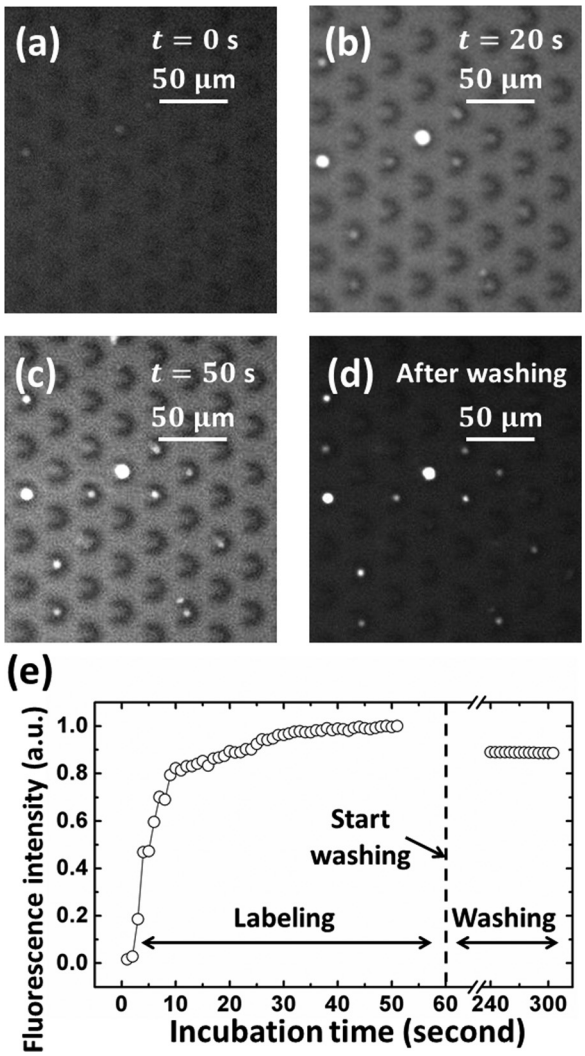

FIG. 4. (a)–(c) Time sequence of on-chip leukocyte labelling with SYTO13 after a load and trap step at an average flow speed of 460 μm/s for 5 min (movie M2 in the supplementary material). An unstained leukocyte sample solution was used, and the images were taken at $t = 0$ s (when labelling solution just arrived in the observed region), 20 s, and 50 s. (d) Fluorescence image of the same point of view after 5 min washing at 460 μm/s. (e) The total fluorescence intensity (sum of fluorescence intensity of each pixel within captured cells) vs. time.

monoclonal antibody fluorescence labels and high resolution microscopies could be used, which was not attempted in this work. The total incubation time was ~1 min for this experiment. After labelling, the leukocytes were washed with wash buffer at 460 μm/s for 5 min [Fig. 4(d)].The background fluorescence noise (intensity outside of the traps) was decreased 10^3 by the wash step [Figs. 4(c) and 4(d)]. Figure 4(e) demonstrates the total fluorescence intensity (the sum of fluorescence intensities of each pixel within the captured leukocytes) of the obtained movies at different incubation times. The total fluorescence intensity initially increased very quickly and began to saturate after ~30 s, consistent with off-chip labelling results.[18]

Leukocyte release

Eight sets of experiments were conducted to investigate the release of leukocytes from the traps. The load step for all the experiments was done at 460 μm/s for 5 min. After the load step, the leukocytes were on-chip incubated for 1 min, 5 min, 10 min, and 20 min and then released at 4.6 mm/s and 9.2 mm/s. Figure 5(a) shows the time sequence of leukocyte release at an average

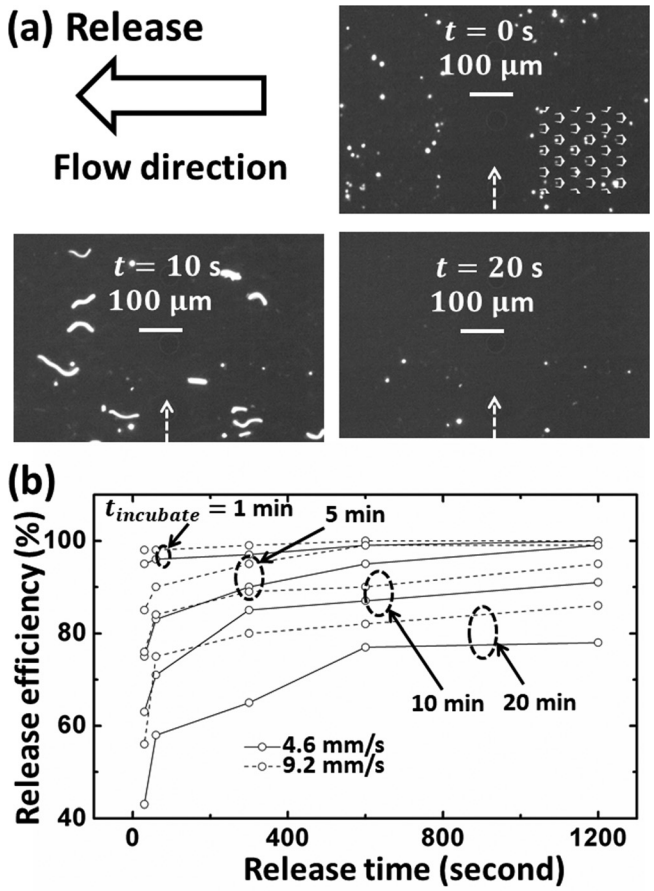

FIG. 5. (a) Time sequence of leukocyte release at an average speed of 4.6 mm/s after a load step at an average flow speed of 460 μm/s for 5 min and an on-chip incubation of 5 min (movie M3 in the supplementary material). A pre-stained leukocyte sample solution was used, and the images are 10 s apart with an exposure time of 10 ms. The left image shows the outlines of traps within 200 μm × 200 μm. (b) Experimental results of release efficiency for different release times after incubation of 1 min, 5 min, 10 min, and 20 min at release flow speeds of 4.6 mm/s and 9.2 mm/s. The dashed arrows point out the location of the row of support pillars. The stripes in the time sequence micrographs are the time-elapse traces of the cells due to the 10 ms exposure time.

speed of 4.6 mm/s after a load step at an average flow speed of 460 μm/s for 5 min and an on-chip incubation for 5 min (movie M3 in the supplementary material). The images are 10 s apart with an exposure time of 10 ms. Figure 5(b) displays the experimental results of percentage of the number of released leukocytes to the number of captured leukocytes, defined as $1\text{-}n_{remain}(t)/n_{ini}$, where $n_{remain}(t)$ is the number of remaining leukocytes at time t and n_{ini} is the number of captured leukocytes at the beginning of the release step. For short incubation time, $\leq$5 min, ~99% of captured leukocytes can be released for both 4.6 mm/s and 9.2 mm/s release flow speeds in 20 min. However, as the incubation time increases, the cells were harder to release, and the higher release flow speed (9.2 mm/s) outperformed a lower 4.6 mm/s release speed. Leukocytes gradually form adhesion bonds to the substrate's surface and to the other cells.[19–21] The adhesion bonds between cells and substrates apparently increase the resistance force when releasing the captured cells. Therefore, higher release flow speed is required for long on-chip incubation. The adhesion bonds between cells make them to aggregate and form clots which cannot be easily released even for high flow speed. During 20 min incubation, 22% and 14% of the total captured leukocytes were not released at 4.6 m/s and 9.2 mm/s, respectively. To the best of our knowledge, there is no previous work studying the leukocyte release efficiency of this type of structures at different on-chip incubation times and flow speeds previously. For the proposed device, the release efficiency of ~99% is better than that reported in the previous work

(70% to 90%)[6] for short incubation time and ~80% for up to 20 min incubation in 20 min release.

Modelling of capture

Previous works have shown that the microfluidic trap devices can capture anywhere from 10% to 90% of the inputted cells.[6,10–12] However, there is a need for models to guide the design of the trap structure design for high capture efficiency. We now provide a qualitative model to better explain the achieved high capture efficiency of microfluidic cell traps.

For modelling of cell trapping, the fluidic circuit model is often discussed.[22,23] Figure 6(a) demonstrates the fluidic circuit model of a trap array. The fluid flux going through the trap and the gap between the traps is F_T and F_G, respectively, and can be calculated as

$$F_T = \frac{\Delta P}{R_T}, \tag{2}$$

$$F_G = \frac{\Delta P}{R_G}, \tag{3}$$

where ΔP is the pressure drop, from one column of traps to the next, and R_T and R_G are the fluidic resistances of the trap structure and the gap, respectively. Two fluxes F_{GG} separating from F_G will join F_T to form a new flux F_G through the next gap.

As discussed in the Device Fabrication and Operation section, the average flow speed ranges from 46 μm/s to 9.2 mm/s and the Reynolds number in the trap region can be calculated as

$$Re = \frac{\rho v_{avg} D_H}{\mu}, \tag{4}$$

where $\rho \approx 1$ g/ml is the density of the fluid, $G_x = 25\,\mu$m is the gap between two traps, $D_H = \frac{2H_{tot}G_x}{H_{tot}+G_x} \approx 22.2\,\mu$m is the hydraulic diameter for critical gaps $G_C = 6\,\mu$m, and $\mu \approx 1 \times 10^{-3}$ Pa·s is the dynamic viscosity of the fluid; Re is of the order of 10^{-3} to 10^{-1}, so viscous forces are dominant and inertial forces can be neglected.[26]

The Péclet number describes the ratio between the advection flow and the diffusion of the particles, which is calculated as

$$pe \frac{v_{avg} L}{D}, \tag{5}$$

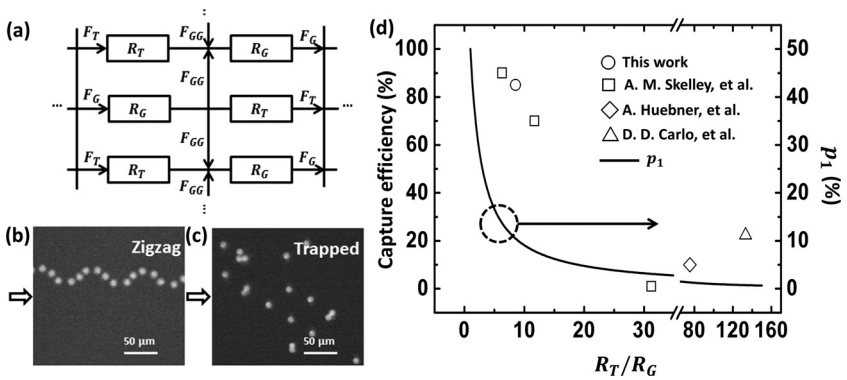

FIG. 6. (a) Fluidic analogous circuit model of the proposed device to explain 2 typical flow patterns of particles: zigzag (always flow in F_{GG}) and trapped (stopped by the microfluidic traps). (b) Trapped 10 μm beads in the device. (c) Integration of 17 frames of fluorescence images of a 10 μm bead following the zigzag trajectory around the microfluidic traps. (d) Experimental results of capture efficiency and the calculated p_1 (solid line, the probability of particles captured by the first column of traps) as a function of R_T/R_G. Open circles: this work; open squares: Ref. 12; open diamond: Ref. 6; and open triangle: Refs. 10 and 11 (assuming 10^6 cells/ml concentration).

where $L = \sqrt{Dt}$ is the characteristic length, $t = P_y/v_{avg}$ is the time fluid flow through the trap region and the gap between two adjacent columns of traps in the y-direction, $D = k_B T/3\pi\mu d_P$ is the diffusion constant of the particles, k_B is the Boltzmann constant, T is the temperature (300 K), and d_P is the particle's diameter. For v_{avg} from 46 μm/s to 9.2 mm/s and $d_P = 10\,\mu$m, *Pé* is of the order of 10^2 to 10^3. The diffusion of the particle is negligible.[25]

Because $Re \ll 1$ and *Pé* $\gg 1$, we can assume that the particle moves at the flow speed of the streamline where the particle center is. Intuitively, if a particle (assuming a size larger than the critical gap) is in flow F_T, it will be captured in the first column [Fig. 6(b), trapped 10 μm beads]. A particle in F_G will not be captured. Therefore, the probability p_1 that a particle is captured in the first column, assuming all empty traps and an uniform distribution of input particles, will just be the probability that the particle moves in F_T

$$p_1 = \frac{F_T}{F_T + F_G} = \frac{1}{1 + \frac{R_T}{R_G}}. \tag{6}$$

The solid line on the right in Fig. 6(d) shows the predicted p_1 for one column of the array for previous work (open circles: this work; open squares: Ref. 12; open diamond: Ref. 6; and open triangle: Refs. 10 and 11 (assuming 10^6 cells/ml concentration)] as a function of R_T/R_G. R_T/R_G was calculated in each case as F_G/F_T within a small part of the total trap arrays using COMSOL software with periodic boundaries applied to avoid computational complexity. The experimental capture efficiencies for entire arrays in each case are also plotted (left axis). The model predicts the trends of higher observed experimental trapping efficiency with small R_T/R_G and low capture efficiency at large R_T/R_G. The experimental numbers for the full arrays are consistently higher of course due to multiple columns in which the particles or cells may be captured.

Note that for regular trap arrays, where each row is vertically displaced from the previous one by 50% of the vertical trap period, if a particle is in the F_{GG} flux, it will wave (zigzag) around from column to column, staying in the gaps to never be captured [Fig. 6(c), an integration of 17 frames of fluorescence images of a 10 μm bead following the zigzag trajectory around the traps]. Such an ideal case rarely occurs for long arrays—as cells are captured, the trap fluidic resistance R_T increases with time in some traps, so that the cells will likely be displaced from the F_{GG} flow and end up in a trap.

We now develop a more sophisticated model and apply it to our geometry. The above model ignores the fact that the particles (of finite size) will interact with the unmovable boundaries when they move against the trap structure. Figure 7 shows the schematic of the flow field at the center plane of the proposed device channel. The streamlines were extracted from COMSOL simulations. The flow within the gap between two adjacent traps can be separated into five regions based on the position of the center of particles: A: the "Trap" region where particles larger than the critical height will flow directly to the trap and get captured; B: the "Wall assisted trap 1" region where particles will hit the boundaries of the trap structure and will be pushed by the flow into the trap; C: the "Zigzag" region where particles will move around the traps and will not be captured; D: the "Wall assisted trap 2" region where particles will flow around the first column of traps but will flow into the "Wall assisted trap 1" region of the next column of traps; E: the "Excluded" region where particles, of non-zero size, cannot exist due to mechanical forces from the outside walls of the trap. When particle's size is large, it will be more likely pushed by the trap boundary into the center "Trap" and "Wall assist trap 1" regions, which will give rise to increased capture efficiency. Due to periodicity, once the particle moves into the "Zigzag" region, it will always follow the zigzag trajectory assuming no particle-to-particle interactions and no diffusion of the particle. Therefore, using symmetry, the probability that a particle gets trapped flowing through the gap G_x is

$$p_2 = 1 - \frac{\int_{z_2}^{z_1} u(x)dx}{\int_0^{G_x/2} u(x)dx}, \tag{7}$$

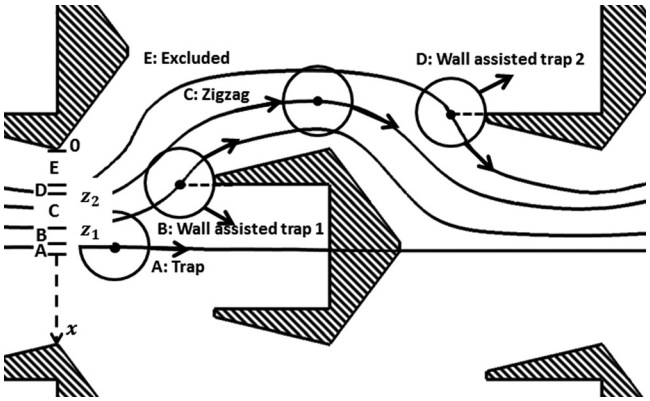

FIG. 7. Schematic of the flow field at the center plane of the proposed device channel. The streamlines were extracted from COMSOL simulations. The fluid flowing through the gap in the x-direction can be separated into 5 regions: "Trap," "Wall assisted trap 1," "Zigzag," "Wall assisted trap 2," and "Excluded." The circles are of 10 μm in diameter.

where z_1 and z_2 are the boundaries of the "Zigzag" region, and $u(x)$ is the flow profile between the gap. Note that particles flowing in the "Excluded" region will be pushed to the "Wall assisted trap 2" region by the trap boundaries. For simplicity, the parabolic flow profile can be used when the Reynolds number is much smaller than 1.[24] The total capture efficiency over two columns can thus be calculated as

$$\eta = p_1 + (1 - p_1)p_2. \tag{8}$$

The first term is the probability that the particle gets trapped by the first column of traps, and the second term is the probability that the particle gets trapped by the next two columns of traps.

Because the flow speeds applied were small, the shear stress induced along the gap was not large enough to significantly deform the leukocytes, which can be confirmed from the observed consistent capture efficiency. The shear stress ranges from about 10^{-3} to 1 Pa for the flow rates tested in this paper. Therefore, we can assume that the leukocytes maintain a spherical conformation flowing through the device. Here, we use a simple geometric approach with this assumption to estimate z_1 and z_2: extending the boundary of the trap structure of $d_P/2$ to a point and then looking back along the streamline from this point to the position z_1 within the gap between two traps. The boundary z_2 can be estimated using the same method as for z_1 (Fig. 7). For the proposed 6 μm critical gap device and using the coordinate setup in Fig. 7, $z_1 = 8.5\,\mu$m and $z_2 = 6.6\,\mu$m. So, the capture efficiency $\eta = 82.6\%$ was calculated using Eq. (8), which is in good agreement with the experiment results.

CONCLUSION

We presented a microfluidic device for on-chip cell chemical processing via capture and release using novel trap structures: streamlined shapes avoiding clogging in capture and release steps and support pillars between two adjacent device units to control the critical gap. A qualitative model was developed to help better understand and design the proposed trap structure array. We demonstrated that a leukocyte capture efficiency of ~84% and a release efficiency of ~99% can be achieved with moderate flow speeds and on-chip incubation times, and a model was presented to explain the device's superior performance. On-chip leukocyte labelling with SYTO13 and washing using the proposed devices showed similar results to conventional off-chip labelling. These results suggest that the device could be used for automated processing to replace many conventional steps for the preparation of cells for flow cytometry, Coulter counting, and other analytical measurements.

SUPPLEMENTARY MATERIAL

See supplementary material for the detailed microfabrication process and micrographs of the fabricated device. **Movie M1:** Loading pre-stained leukocytes into a 6-μm critical gap trap array at an average flow speed of 460 μm/s. **Movie M2:** On-chip labelling of the unstained leukocyte sample via flowing SYTO13 labelling solution (25 μM) at an average flow speed of 460 μm/s after a load and trap step of the same average flow speed for 5 min. **Movie M3:** Release of the pre-stained leukocyte sample at an average flow speed of 4.6 mm/s after a load step at an average flow speed of 460 μm/s for 5 min and an on-chip incubation of 5 min. Note that the stripes in the movies are the time-lapse traces of cells due to the 10 ms exposure time of each frame.

ACKNOWLEDGMENTS

This work was funded by a NCI/NIH STTR Award (Project No. R42CA174121) and GPB Inc.

[1]M. Toner and D. Irimia, Annu. Rev. Biomed. Eng. **7**, 77–103 (2005).
[2]J. Nguyen, Y. Wei, Y. Zheng, C. Wang, and Y. Sun, Lab Chip **15**, 1533–1544 (2015).
[3]A. J. Mach, J. H. Kim, A. Arshi, S. C. Hur, and D. Di Carlo, Lab Chip **11**, 2827–2834 (2011).
[4]K. J. Morton, K. Loutherback, D. W. Inglis, O. K. Tsui, J. C. Sturm, S. Y. Chou, and R. H. Austin, Lab Chip **8**, 1448–1453 (2008).
[5]Y. Chen, J. D'Silva, R. H. Austin, and J. C. Sturm, Biomicrofluidics **9**(5), 054105 (2015).
[6]A. Huebner, D. Bratton, G. Whyte, M. Yang, A. J. deMello, C. Abell, and F. Hollfelder, Lab Chip **9**(5), 692–698 (2009).
[7]D. Jin, B. Deng, J. X. Li, W. Cai, L. Tu, J. Chen, Q. Wu, and W. H. Wang, Biomicrofluidics **9**, 014101 (2015).
[8]F. Yesilkoy, R. Ueno, B. X. E. Desbiolles, M. Grisi, Y. Sakai, B. J. Kim, and J. Brugger, Biomicrofluidics **10**, 014120 (2016).
[9]L. Mi, L. Huang, J. X. Li, G. Q. Xu, Q. Wu, and W. H. Wang, Lab Chip **16**, 4507 (2016).
[10]D. Di Carlo, N. Aghdam, and L. P. Lee, Anal. Chem. **78**, 4925–4930 (2006).
[11]D. Di Carlo, L. Y. Wu, and L. P. Lee, Lab Chip **6**, 1445–1449 (2006).
[12]A. M. Skelley, O. Kirak, H. Suh, R. Jaenisch, and J. Voldman, Nat. Methods **6**, 147–152 (2009).
[13]P. R. Wheater, H. G. Burkitt, and V. G. Daniels, *Functional Histology. A Text and Colour Atlas* (Churchill Livingstone, Edinburgh, 1979).
[14]S. Park, R. R. Ang, S. P. Duffy, J. Bazov, K. N. Chi, P. C. Black, and H. Ma, PLoS One **9**(1), e85264 (2014).
[15]H. K. Lin, S. Zheng, A. J. Williams, M. Balic, S. Groshen, H. I. Scher, M. Fleisher, W. Stadler, R. H. Datar, Y.-C. Tai, and R. J. Cote, Clin. Cancer Res. **16**, 5011–5018 (2010).
[16]T. M. H. Lee, D. H. Y. Lee, C. Y. N. Liaw, A. I. K. Lao, and I. M. Hsing, Sens. Actuators, A **86**(1), 103–107 (2000).
[17]A. Sharei, J. Zoldan, A. Adamo, W. Y. Sim, N. Cho, E. Jackson, S. Mao, S. Schneider, M.-J. Han, A. Lytton-Jean, P. A. Basto, S. Jhunjhunwala, J. Lee, D. A. Heller, J. W. Kang, G. C. Hartoularos, K.-S. Kim, D. G. Anderson, R. Langer, and K. F. Jensen, Proc. Natl. Acad. Sci. U.S.A **110**, 2082–2087 (2013).
[18]P. Lebaron, N. Parthuisot, and P. Catala, Appl. Environ. Microbiol. **64**(5), 1725–1730 (1998), http://aem.asm.org/content/64/5/1725.abstract.
[19]D. A. Hammer and S. M. Apte, Biophys. J. **63**, 35–57 (1992).
[20]C. Dong and X. X. Lei, J. Biomech. **33**(1), 35–43 (2000).
[21]S. I. Simon and H. L. Goldsmith, Ann. Biomed. Eng. **30**, 315–332 (2002).
[22]W. H. Tan and S. Takeuchi, Proc. Natl. Acad. Sci. U.S.A. **104**, 1146–1151 (2007).
[23]A. Karimi, S. Yazdi, and A. M. Ardekani, Biomicrofluidics **7**, 021501 (2013).
[24]E. M. Purcell, Am. J. Phys. **45**, 3 (1977).
[25]H. Wang, P. Iovenitti, E. Harvey, and S. Masood, Smart Mater. Struct. **11**(5), 662 (2002).
[26]J. P. Brody, P. Yager, R. E. Goldstein, and R. H. Austin, Biophys. J. **71**, 3430–3441 (1996).